Petroleum Science 23 (2026) 2723–2734

Contents lists available at ScienceDirect

Petroleum Science

journal homepage: www.keaipublishing.com/en/journals/petroleum-science

Original Paper

Effects of salinity variations on shale imbibition behavior: Insights into the microscopic mechanisms

Xuan-Zhe Xia [a], Ting Chen [b], Han Wang [a], Yu-Xuan Xia [a], Liang Luo [c,*], Jian-Chao Cai [a,**]

[a] State Key Laboratory of Petroleum Resources and Engineering, China University of Petroleum (Beijing), Beijing, 102249, China
[b] Exploration and Development Research Institute of Shengli Oilfield Company, Sinopec, Dongying, 257015, Shandong, China
[c] College of Physics and Electronics, Hunan Institute of Science and Technology, Yueyang, 414000, Hunan, China

ARTICLE INFO

Article history:
Received 22 December 2025
Received in revised form
9 February 2026
Accepted 31 March 2026
Available online 4 April 2026

Edited by Meng-Jiao Zhou

Keywords:
Shale imbibition
Salinity
Nuclear magnetic resonance
Clay swelling
Lattice Boltzmann method

ABSTRACT

Shale reservoirs contain abundant micro/nanoscale pores, which facilitate capillarity-dominated imbibition as an effective mechanism for enhancing hydrocarbon recovery. During hydraulic fracturing, the penetration of low salinity fracturing fluids can induce clay hydration and swelling, leading to pore structure alterations. However, the effects on imbibition behavior remain insufficiently understood. In this study, high temperature and high pressure imbibition experiments coupled with nuclear magnetic resonance are performed on continental shale. Furthermore, the structural and mineralogical evolution of shale following interaction with deionized water is evaluated by scanning electron microscope. Finally, the pore fracture structure model incorporating clay swelling is constructed and the flow of fracturing fluids is simulated by the lattice Boltzmann method. The results indicate that cores exhibit greater imbibition recovery at higher salinity. The recovery shows a strong positive correlation with pore structure, with denser and less connected pores leading to reduced recovery. Exposed to deionized water, clay is observed to swell and compress both pore space and fracture. After swelling, the flow channels in the two-dimensional model are narrowed or even closed, resulting in fewer effective flow pathways and a reduced swept zone of the oil phase. Meanwhile, the oil phase is prone to snap-off, producing discontinuous droplets that disperse within the pore space. This ultimately leads to a reduction in imbibition recovery after swelling. High salinity effectively suppresses clay mineral swelling and preserves the original pore structure, thereby resulting in higher imbibition recovery. Understanding the imbibition mechanisms under different salinity provides valuable insights for the design of hydraulic fracturing in oilfield applications.

1. Introduction

China contains substantial shale oil and gas resources, primarily distributed in representative basins such as the Sichuan, Ordos, and Bohai Bay basins. These unconventional resources serve as a crucial energy reserve to succeed increasingly depleted conventional hydrocarbon reservoirs (Zhao et al., 2020; Fu et al., 2024). However, due to the compact pore structure, poor connectivity, and strong heterogeneity of shale reservoirs, hydraulic fracturing remains the most effective technique for their development (Middleton et al., 2017; Sun et al., 2024; Zheng et al., 2025). During the shut-in period, fracturing fluids are driven by capillary forces into the shale matrix, displacing hydrocarbons and enhancing production (Eltahan et al., 2021; Zhang et al., 2024). This process, in which the wetting phase invades the porous medium under capillary forces and displaces the non-wetting phase, is referred to as imbibition (Li et al., 2022; Ashraf et al., 2023). In contrast to other reservoir types, shale formations are rich in clay minerals with semipermeable membrane properties. When a salinity gradient exists between the internal and external fluids, the semipermeable membrane permits the passage of water molecules but restricts the transport of salt ions (Fritz, 1986; Wang et al., 2025a). The influx of water increases the interlayer spacing of clay minerals, resulting in hydration induced swelling that

* Corresponding author.
** Corresponding author.
E-mail addresses: fuboyi314@gmail.com (L. Luo), caijc@cup.edu.cn (J.-C. Cai).
Peer review under the responsibility of China University of Petroleum (Beijing).

https://doi.org/10.1016/j.petsci.2026.03.066

threatens the structural stability of shale reservoirs (Anderson et al., 2010; Mu et al., 2025). However, low salinity fracturing fluids can easily trigger shale hydration, which alters the native pore structure and subsequently complicates subsequent imbibition (Khan et al., 2021; Shao et al., 2023). Therefore, investigating the imbibition behavior and underlying mechanisms of fracturing fluids with different salinities is crucial for enhancing shale oil and gas recovery and provides guidance for selecting appropriate salinity in field operations.

Currently, several researchers have investigated shale reservoir imbibition behavior through theoretical modeling, numerical simulations, and core experiments. Lucas and Washburn proposed the LW equation, based on the Hagen–Poiseuille law, to describe the evolution of the fluid imbibition front within capillaries (Lucas, 1918; Washburn, 1921). Numerous imbibition theories have been developed from the LW equation, but they rely on the assumption of linear flow paths and ignore the curved streamlines in real porous media. By applying fractal theory to capture the tortuosity and pore structure characteristics of complex shale pore structure, the LW equation can be modified to better reflect the flow behavior within shale reservoirs (Cai et al., 2014; Zhang et al., 2025). The Handy model (Handy, 1960) and Scaling model (Mattax and Kyte, 1962) have also been applied to characterize imbibition, but their idealized assumptions constrain their use in real reservoirs. Furthermore, hydration induced changes in pore structure pose challenges for mathematical modeling.

Pore-scale simulation methods can intuitively reveal the fluid imbibition mechanisms within porous media at the microscopic perspective. Molecular simulation, which accounts for actual intermolecular forces, provides a precise description of fluid-fluid interaction mechanisms. However, it is highly computationally demanding and usually restricted to nanoscale simulations (Huang et al., 2024; Wang et al., 2024; Qin et al., 2025). The pore network model, with high computational efficiency, cannot capture complex pore structure features or fluid-solid interactions due to structural simplifications. Additionally, the accuracy of this method requires further validation. The lattice Boltzmann method (LBM), a mesoscopic direct numerical simulation approach, has advantages in independent of mesh generation, parallelization, and avoiding complex explicit fluid interface tracking algorithm. It has been widely applied to study fluid flow patterns, interface evolution, and distribution characteristics within the complex porous media (Zhao et al., 2023; Munarin et al., 2025).

Combining multiple characterization techniques, core scale imbibition experiments provide an effective method to investigate complex imbibition behavior within the pore spaces of shale. Imbibition curves can be readily obtained via recording the volume or mass of fluid imbibed by the cores (Zuo et al., 2024). However, in tight unconventional reservoirs, the variations in fluid volume or mass during imbibition are typically minimal, which hinders precise quantification (Yao et al., 2021). By quantifying the differential X-ray attenuation of distinct materials, X-ray computed tomography employs inversion algorithms to reconstruct the three-dimensional structure of porous media and reveal the internal fluid distribution (Wang et al., 2019). But obtaining high resolution X-ray computed tomography images typically requires small size samples (Peng and Xiao, 2017), Which makes it difficult to avoid flow disturbances induced by end effects.

Nuclear magnetic resonance (NMR), by capturing the decay response of hydrogen nuclei in porous media and applying numerical inversion methods, provides a rapid and nondestructive means of determining internal fluid distributions (Maillet et al., 2022; Dou et al., 2024; Wang et al., 2025b). NMR has enabled researchers to explore how boundary conditions, flow modes, wettability, and fractures affect fluid imbibition behavior. Lyu et al. (2019) used NMR measurements at ambient temperature and pressure to examine the imbibition behavior of tight sandstone under various boundary conditions. Their results indicate that radial flow along the cylindrical surface and linear flow from the core ends interact during the late stage of imbibition, leading to the reduced recovery observed in fully open cores. Wu et al. (2024) investigated imbibition within the multiscale pore throat network of tight sandy conglomerates. They divide the imbibition process into three distinct stages: suction, diffusion, and stabilization. The movement of oil from micropores to larger pores under capillary forces is recognized as a critical mechanism contributing to increased recovery. Using $MnCl_2$ solutions to shield the NMR signal of the water phase, Lin et al. (2024) demonstrated that the water initially enters hydrophilic micropores of lacustrine shale, driving oil into oil-wet mesopores. This oil is subsequently mobilized by capillary forces from the mesopores into microfractures and ultimately expelled. Micropores with weakly water-wet or mixed-wet properties exert a significant control on shale oil recovery. Liu and Sheng (2020) found that the imbibition distance within tight reservoirs is extremely short by NMR, requiring numerous fractures to generate sufficient imbibition interfaces to enhance recovery at the reservoir scale.

The modification of pore structures resulting from clay hydration similarly impacts imbibition processes. Yang et al. (2018) reported that the evolution of transverse relaxation time (T_2) spectra during imbibition differs among shale lithofacies. Hydration in marine shales produces connected microfractures, which shift the T_2 spectra toward larger pores and accelerate imbibition. In continental shale, matrix pore damage causes T_2 values to decrease gradually, thereby lowering the water imbibition rate. The influence of hydration induced particle blockage and fracture extension, two contrasting mechanisms, on imbibition behavior is still not well understood (Meng et al., 2015; Shen et al., 2016; Yang et al., 2023). Fracturing fluids within shale reservoirs possess inherent pressure, whereas most existing imbibition experiments are carried out at ambient conditions. Consequently, it is necessary to perform shale imbibition experiments under high temperature and pressure conditions.

To investigate the mechanisms by which variations in fluid salinity affect shale imbibition behavior, continental shale samples are selected in this study. First, the basic physical properties and mineral composition of the cores are characterized to provide a foundation for subsequent experiments. Next, using NMR, shale imbibition experiments are conducted under high temperature and high pressure conditions with solutions of different salinities. Then, the imbibition behavior and influencing factors are analyzed. Finally, based on scanning electron microscope (SEM) characterization and LBM simulations, the microscopic mechanisms governing the influence of fluid mineralization variations on shale imbibition behavior are elucidated.

2. Materials and methodology

2.1. Samples

In this work, seven shale samples from the Shahejie Formation are selected. The porosity of the shale samples is determined using Boyle's law, and their permeability is measured with the pulse-decay method (Table 1). The first four samples, obtained from a single well, have an average porosity of 2.2792% and an average permeability of 0.0043×10^{-3} μm^2. The remaining three samples originate from a different well, with an average porosity of 3.2804% and an average permeability of 0.0060×10^{-3} μm^2. Following drying and impurity removal, the shale samples are ground to 200-mesh powder, and their mineral compositions are

Table 1
The porosity and permeability of the collected shale samples.

No.	Depth, m	Porosity, %	Permeability, × 10^{-3} μm^2
B37	3453.80	2.1425	0.0032
B44	3461.30	1.0733	0.0010
B48	3465.88	3.1648	0.0053
B128	3556.00	2.7362	0.0076
314	3793.00	0.5369	0.0025
421	3847.20	1.6510	0.0014
527	3934.90	7.6532	0.0141

evaluated by X-ray Diffraction. The shale samples are dominated by clay minerals and carbonates, with illite and illite/smectite mixed layers (I/S) serving as the major clay constituents (Fig. 1).

2.2. Imbibition experiment based on NMR

Relaxation theory establishes the relationship between transverse relaxation time (T_2) and the pore structure of porous media, providing a theoretical foundation for the application of NMR in fluid flow within different pores. Throughout the experiment, the magnetic field strength is maintained uniformly, and the influence of diffusion relaxation is negligible. Moreover, shale is enriched with micro/nanopores, where the bulk relaxation of the confined fluids is weak. Therefore, surface relaxation constitutes the dominant relaxation mechanism within the pore space. The surface relaxation process is governed by the interaction strength between the rock surfaces and the fluid, as well as the characteristics of the pore structure. Finally, the T_2 can be expressed as (Mitra et al., 1992):

$$\frac{1}{T_2}=\rho\frac{S}{V} \tag{1}$$

where ρ denotes the surface relaxivity influenced significantly by paramagnetic substances, S represents the pore surface area, and V denotes the pore volume.

The logarithmic mean of T_2 (T_{2LM}) is used to quantitatively evaluate the average pore structure characteristics, and the calculation procedure as follows:

$$T_{2LM}=e^{\left(\sum_{T_{2min}}^{T_{2max}}(A_i/A_{Total})\ln T_{2i}\right)} \tag{2}$$

where T_{2min} and T_{2max} indicate the minimum and maximum transverse relaxation times, respectively. T_{2i} is defined as the i-th relaxation component within this interval between T_{2min} and T_{2max}, A_i denotes its corresponding amplitude, and A_{Total} refers to the accumulative signal amplitude of the shale sample.

Deuterium oxide (D_2O), which does not exhibit an NMR signal, is used as the wetting phase in the imbibition experiments to achieve unambiguous signal separation from the non-wetting phase. Based on the composition of formation water from the studied stratigraphic layers, various mass concentration (0%, 4%, 7%, and 14%) of saline solutions are prepared using NaCl, KCl, $CaCl_2$, $MgCl_2$, and D_2O (Table 2). In addition, the salinity of the imbibition fluids corresponding to each sample is also listed. Sample 314, saturated with oil, is placed in a 14% solution for 40 h to undergo imbibition. The sample is then removed and transferred to a 7% salinity solution, where imbibition is continued until 88 h. Subsequently, the sample is taken out again and immersed in a 4% salinity solution until 136 h. Finally, the sample is transferred to a 0% salinity solution, where imbibition is conducted until 184 h. During each transfer, the sample is wrapped with plastic film to prevent fluid evaporation. Next, the interfacial tension between saline solutions with different concentrations and white oil is measured. After the samples are washed and dried, the contact angles of the shale/saline solutions/white oil are measured (Fig. 2(a)). Subsequently, the samples are saturated with white oil at 30 MPa for three days to ensure that the oil fully filled the pore spaces. After saturation, the T_2 spectra of the cores are evaluated. Finally, the samples are placed in a vessel filled with saline solutions of the corresponding concentrations. Under 70 °C and 30 MPa, the T_2 spectra are acquired at different imbibition times to investigate the shale imbibition behavior (Fig. 2(b)).

Table 2
Composition of the imbibition fluid.

No.	Salinity	Mass, g				
		NaCl	KCl	$MgCl_2$	$CaCl_2$	D_2O
B128	14%	109.3	4.1	3.7	22.9	860
B48	7%	54.65	2.05	1.85	11.45	930
B44	0%	/	/	/	/	1000
527	7%	54.65	2.05	1.85	11.45	930
421	0%	/	/	/	/	1000
314	14%	109.3	4.1	3.7	22.9	860
	7%	54.65	2.05	1.85	11.45	930
	4%	31.23	1.17	1.06	6.54	960
	0%	/	/	/	/	1000

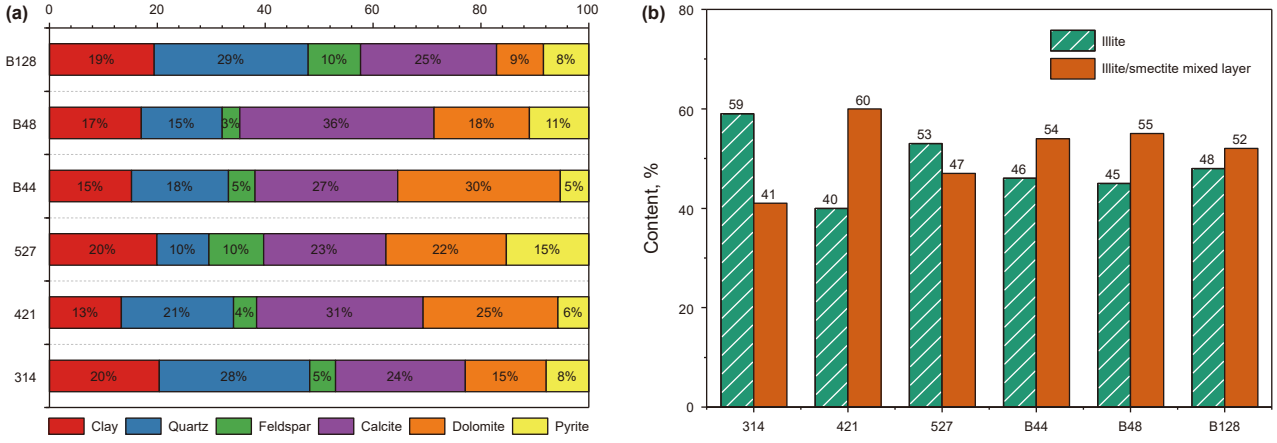

Fig. 1. Mineral composition of shale. **(a)** Mineral content, **(b)** clay types.

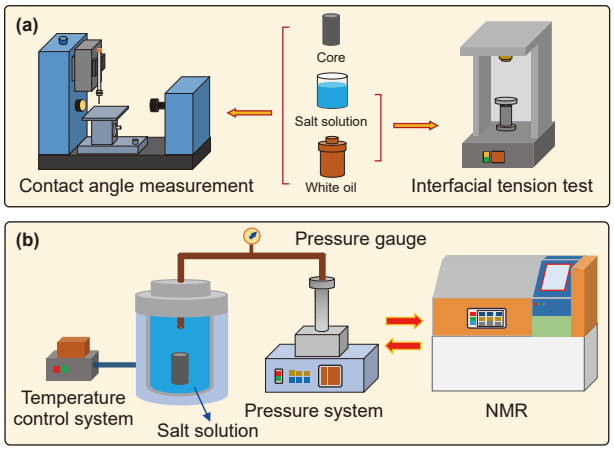

Fig. 2. Experimental flowchart. **(a)** Contact angle and interface tension test, **(b)** imbibition experiment based on NMR.

3. Results

3.1. T_2 spectra of imbibition

Based on their profiles, the T_2 spectra of saturated shale can be categorized into two types: unimodal and bimodal. The T_2 spectrum of Sample 421 exhibits a unimodal distribution (Fig. 3(b)), indicating a uniform and weakly complex pore structure, whereas the remaining samples display bimodal characteristics. The saturated T_2 spectrum of Sample 527 differs from those of the other bimodal cores in that its right peak is significantly higher than the left (Fig. 3(d)), indicating a larger proportion of macropores. This observation is consistent with the high porosity and permeability of Sample 527. Furthermore, the correlations of T_{2LM} with porosity and permeability are established separately (Fig. 4). T_{2LM} shows strong positive correlations with both porosity and permeability. Therefore, a larger T_{2LM} reflects the presence of abundant macropores and good pore connectivity, indicating favorable reservoir quality.

During imbibition, the saline solution enters the pore space under capillary forces and displaces the oil phase. This process reduces the NMR signal amplitude of the samples, as reflected by the decreased envelope area of the NMR curves. The magnitude of T_2 is proportional to pore size, implying that smaller T_2 values correspond to smaller pores. For B44, B48, and B128, with similar T_{2LM} values, the three cores exhibit a decrease in amplitude within the 0–1 ms range (Fig. 3(a), (c), and (e)). The enhanced capillary forces acting on the wetting phase within smaller pores promote preferential imbibition in these pores. Consequently, the salt solution continues to invade the small pores and displace the oil phase until equilibrium is reached. Similarly, Samples 421 and 314 show similar amplitude variations within 0–1 ms (Fig. 3(b) and (f)). However, all shale samples (except for Sample 527) exhibit a slight increase in amplitude within 1–100 ms, which corresponds to larger pore sizes. Oil mobilized from small pores by capillary forces flows into larger pores with lower entry resistance, resulting in an increase in signal intensity within larger pores.

In contrast, Sample 527 exhibits a continuous decrease in amplitude over the 0-10,000 ms range during imbibition, ultimately stabilizing at equilibrium stage. At 4 h, Sample 527 displays a signal at 300 ms that fluctuates during the subsequent imbibition period, and this phenomenon is not observed in the other samples. This can be attributed to microcracks on the surface of Sample 527, where fluid enters and generates NMR signals (Fig. 3(d)). The formation of microfractures creates preferential pathways for fluid flow, facilitating rapid fluid imbibition. This process further promotes the expansion of microfractures and the development of a fracture network. Therefore, the oil within Sample 527 is rapidly discharged, resulting in a pronounced rightward shift of the T_2 spectrum.

3.2. Imbibition recovery

The T_2 spectra from NMR allow quantification of the oil phase signal in shale, and the oil content acquired at different imbibition times reveals the evolution of recovery (Fig. 5). Higher salinity is associated with improved recovery (Fig. 5(a)). In deionized water, clay minerals exhibit the strongest hydration capacity. This reduces pore space through hydration stress and narrows the flow pathways, ultimately resulting in the lowest recovery of B44. B48 and B44 exhibit similar pore structure characteristics, and the partial suppression of clay swelling by 7% brine allows B48 to achieve a faster recovery increase during the early stage of imbibition. However, in the later stage of imbibition, particle migration induced by clay swelling can block flow pathways, slowing the increase in recovery for B48. For B128, clay hydration is effectively suppressed under high salinity solution (Murtaza et al., 2024). Combined with its inherently high permeability, these factors result in the highest final recovery.

The presence of an interconnected microfractures system in Sample 527 substantially enhances the contact area with the invading fluid. This reduces the negative impact of clay particle blockage, resulting in a markedly higher recovery compared with the other samples lacking microfractures (Fig. 5(b)). Within the first 40 h, the 14% solution effectively maintains pore connectivity, leading to a rapid rise in recovery for Sample 314. As the salinity of the fluid progressively decreases, the associated alterations in pore structure weaken the imbibition, thereby slowing the subsequent growth in recovery. The relatively high salinity in the early stage stabilizes the pore structure, resulting in a higher final recovery for Sample 314 compared with Sample 421.

4. Discussion

4.1. Effect of wettability and interfacial tension on recovery

The wettability and interfacial tension of solution systems with different salinities are also measured, as shown in Fig. 6. Increasing salinity weakens the water-rock interaction, as reflected by a larger contact angle, making the rock surface more oil-wet (Fig. 6(a)). Salinity also affects interfacial tension, which is slightly elevated at higher salinity (Fig. 6(b)). Capillary forces, governed by the contact angle (θ) and interfacial tension (σ) according to the Laplace equation, directly control fluid imbibition behavior. Therefore, the $\sigma\cdot\cos\theta$ values of the different samples are obtained (Fig. 6(c)). The weak correlation is observed between $\sigma\cdot\cos\theta$ and imbibition recovery ($R^2 = 0.11$). This indicates that, within the salinity range investigated, wettability and interfacial tension have a limited effect on imbibition recovery. As a result, they cannot adequately explain the observed variations in recovery under different salinity conditions. In addition to the properties of the rock surface and fluid characteristics, the relationship between the pore structure features of shale samples and recovery is also worth analyzing.

4.2. Correlations between pore structure and imbibition recovery

Pore structure characteristics also impact on the imbibition recovery of shale samples. The relationship between T_{2LM} and imbibition recovery is established, which indicates that T_{2LM} is positively correlated with recovery (Fig. 7(a)). This demonstrates

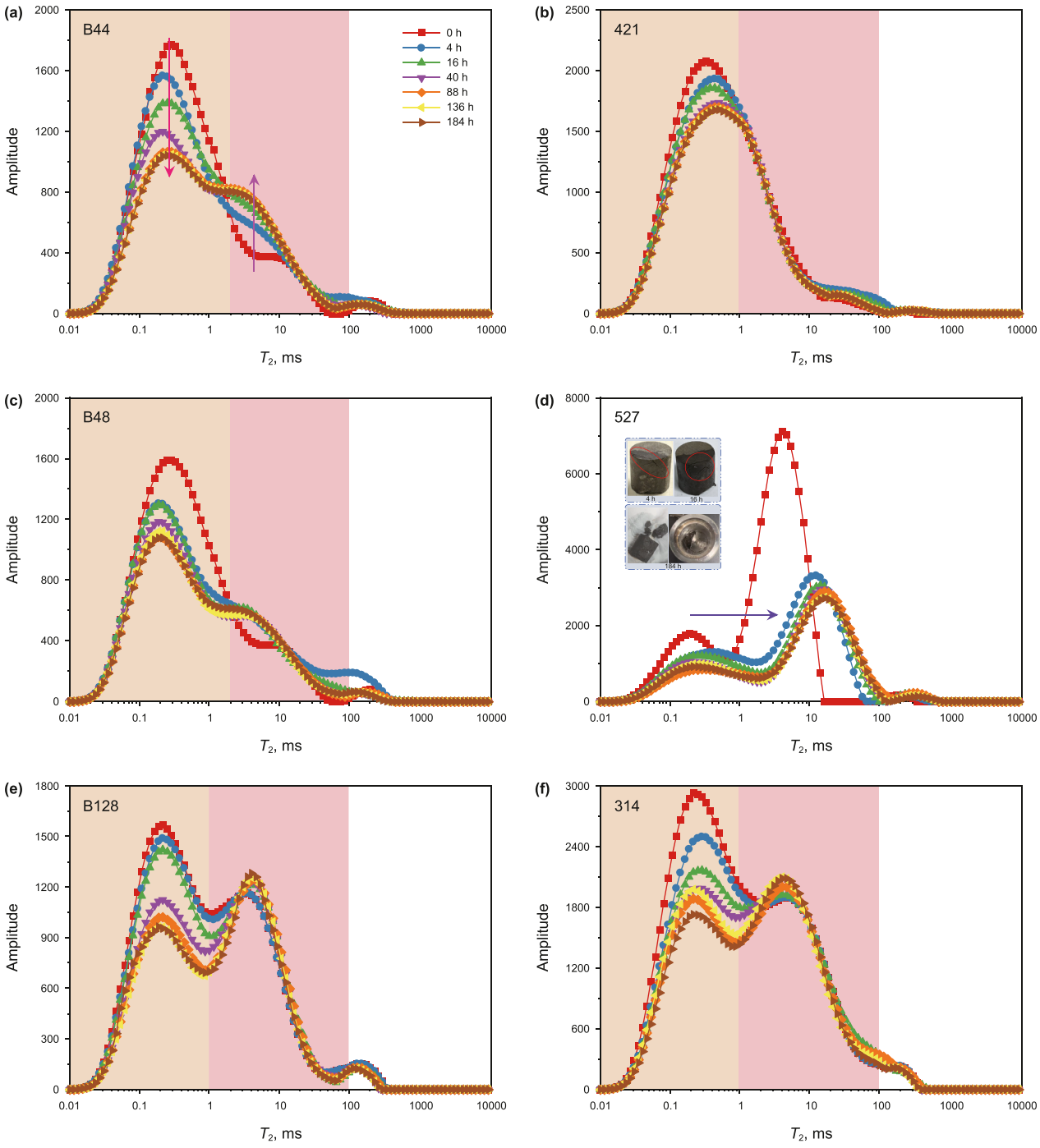

Fig. 3. The T_2 spectrum distributions at different imbibition times. **(a)** B44, **(b)** 421, **(c)** B48, **(d)** 527, **(e)** B128, **(f)** 314.

that pore size has a significant impact on imbibition recovery: smaller pores hinder fluid imbibition, whereas larger pores are more conducive. In addition, 40 h is the turning point for imbibition rate. Therefore, data from the first 40 h are fitted to determine the imbibition velocity, and the relationship between imbibition velocity and T_{2LM} is subsequently plotted (Fig. 7(b)). T_{2LM} shows a clear positive relationship with imbibition velocity, with higher T_{2LM} indicating larger pores and faster imbibition rate. The pore volume of the shale samples is quantified using gas porosity measurements. The results indicate a clear positive correlation between pore volume and both recovery and imbibition velocity (Fig. 7(c) and (d)). This implies that favorable rock physical properties facilitate fluid imbibition and improve imbibition efficiency. The clay hydration induced swelling diminishes pore size and compromises the pore structure, ultimately resulting in slower imbibition rate and lower recovery. At low salinity conditions, stronger clay swelling exerts greater constriction on pore space and flow pathways. This also reveals that the fundamental difference in imbibition performance under different salinity conditions is determined by the degree of pore structure alteration induced

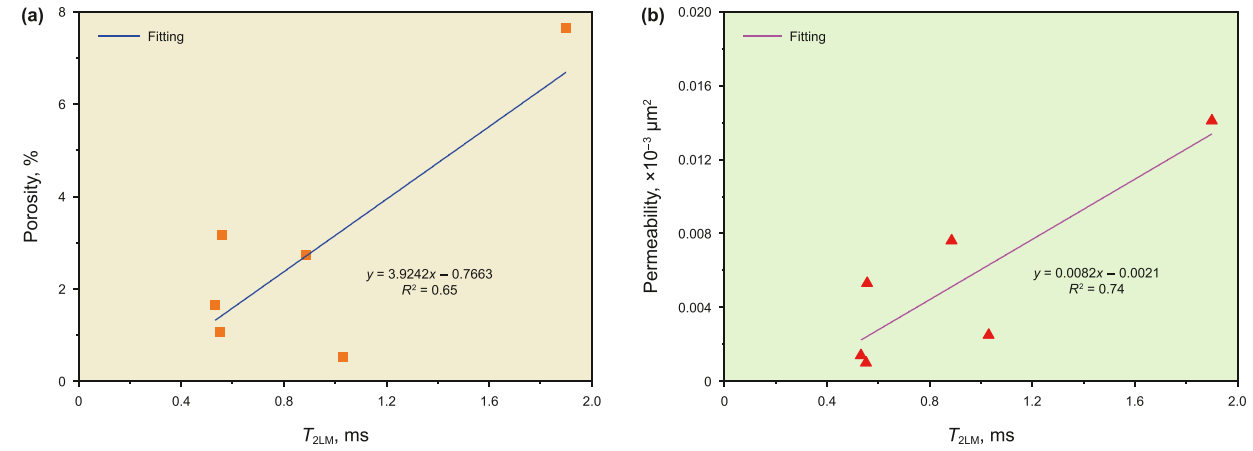

Fig. 4. The correlation of T_{2LM} with **(a)** porosity and **(b)** permeability.

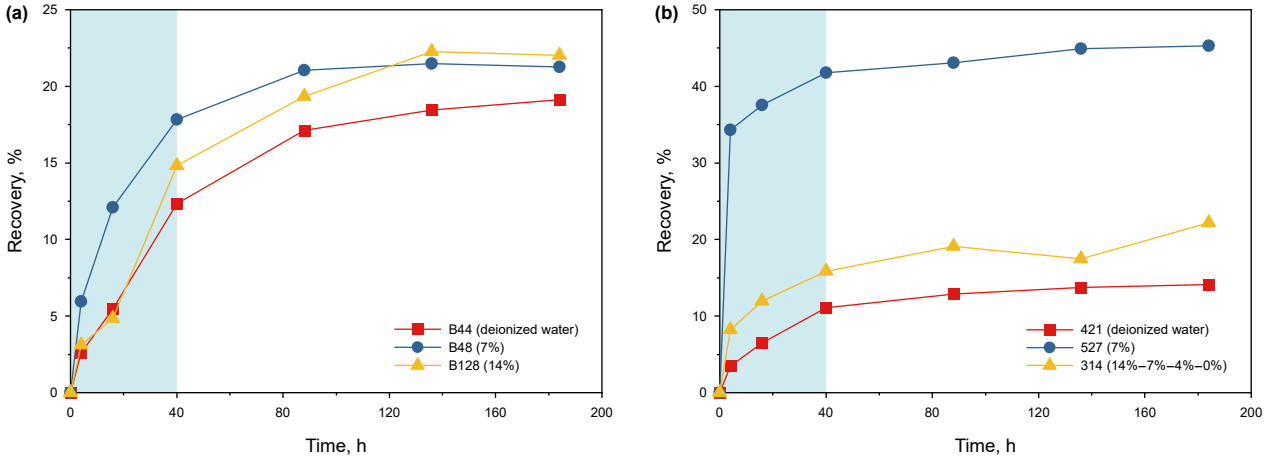

Fig. 5. Imbibition recovery. **(a)** B44, B48, B128, **(b)** 421, 527, 314.

by clay hydration. Therefore, it is necessary to further elucidate, at the microscopic scale, the mechanisms by which structural alterations influence fluid imbibition.

4.3. Microscopic mechanisms of imbibition under pore structure alterations

4.3.1. Characterization of clay swelling

To confirm clay mineral swelling under low salinity conditions, SEM and energy dispersive spectroscopy (EDS) are used to characterize shale microstructure and mineral distribution before and after immersion in deionized water. Using wire cutting, continental shale sample from the Shahejie Formation is prepared as cubic slices with dimensions of 1 cm × 1 cm × 0.5 cm. The slice is subsequently mechanically polished and argon ion polished to obtain a smooth surface. After carbon coating to enhance conductivity, the sample is inserted into the ZEISS Merlin SEM (Fig. 8(a)). Before immersion, the samples contain abundant carbonate and clay minerals, with only a limited number of isolated pores and microfractures observed (Fig. 8(b) and (c)). The hydration behavior of I/S mixed layers reflects contributions from both illite and smectite (Wang et al., 2020). Illite is associated with high hydration stress but limited volumetric expansion, while smectite exhibits significant swelling. After 5 days of interaction with deionized water at 70 °C and 30 MPa, passivation of particle edges induced by clay mineral swelling is observed, consistent with Zeng et al. (2021). The nearby pore spaces are compressed, leading to pore closure and blockage (red area, Fig. 8(c) and (f)). Combined with the EDS, a clear reduction in carbonate minerals is found after immersion (Fig. 8(e)). Although carbonate minerals dissolve to form abundant secondary dissolution pores, their disconnected nature prevents any effective enhancement of fluid flow. Conversely, detached carbonate particles may obstruct pore throat channels and thereby restrict fluid flow. Microfractures also undergo closure caused by hydration swelling, reducing fracture width and increasing flow resistance within the fractures (Fig. 8(d) and (g)). This result is consistent with the conclusions reported by Sui et al. (2018). In summary, SEM observations clearly confirm that interactions between shale and deionized water induce significant changes in pore structure. Swelling of clay minerals results in constricted or completely blocked flow pathways. The phenomena founded by SEM provide a basis for constructing porous media models that incorporate clay swelling. Furthermore, pore fracture models before and after clay mineral swelling are established. And the LBM is employed to simulate fluid imbibition in the porous medium.

4.3.2. Two-dimensional pore structure model

The modular automated processing system is employed to acquire a high-resolution image (2.099 mm × 0.888 mm) form B37 with wide field of view. A specific region of interest

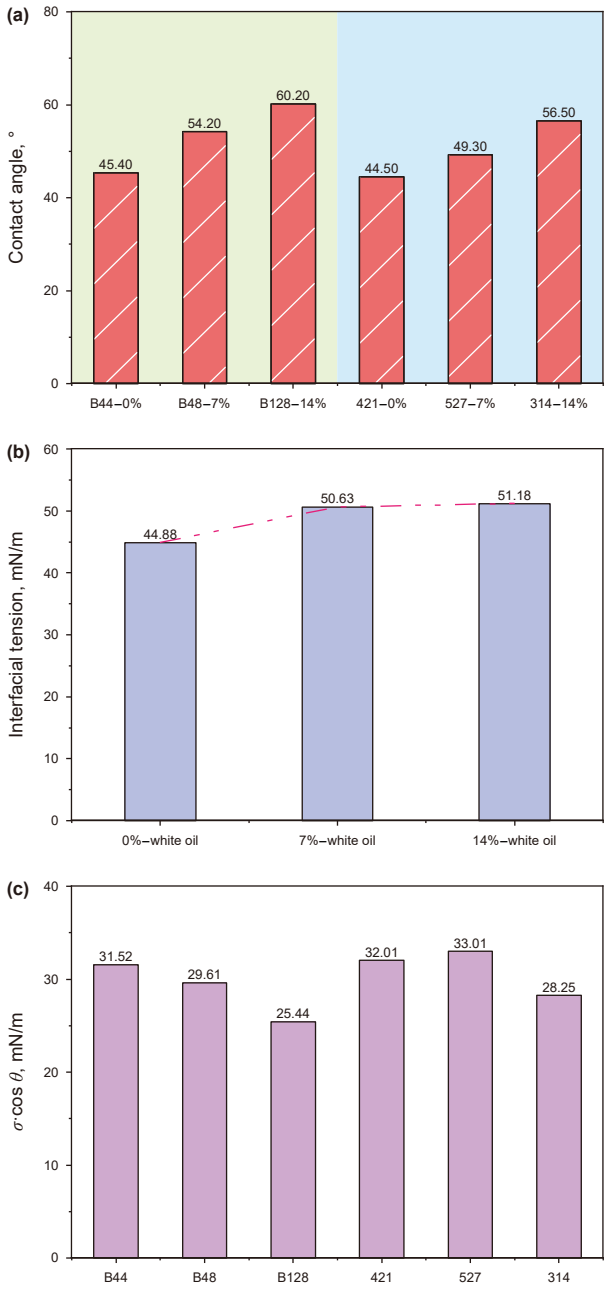

Fig. 6. Wettability and interfacial tension of brine systems with varying salinity. **(a)** Contact angle, **(b)** interface tension, **(c)** σ·cos θ.

(40 μm × 28 μm) is selected from the wide field of view image, and its pore fracture features are extracted using median filtering and threshold segmentation. Subsequently, the watershed algorithm is applied to delineate the throats, thereby reconstructing the original two-dimensional pore fracture network (Fig. 9(a)). By controlling the morphological changes of clay minerals, their swelling can intrude into and erode the pore space, thereby reflecting the impact of clay hydration on pore structure. The red regions in Fig. 9(b) illustrate the extent of clay mineral swelling. The pore fracture structure after clay swelling is presented by Fig. 9(c). It can be observed that swelling compresses the pore space, leading to a reduction in available flow pathways.

4.3.3. LBM simulation

Pore-scale simulations provide a direct and intuitive perspective for revealing microscale flow behavior, fluid distribution, and the evolution of fluid interfaces. In traditional computational fluid dynamics approaches, the tortuous and highly irregular pore fracture geometry of porous media complicates mesh generation, and identifying fluid interfaces requires the additional use of complex interface tracking algorithms. In contrast to methods that numerically solve the Navier-Stokes equations, the LBM employs a particle-based representation in which fluid particles occupy lattice nodes discretized by the physical space. Fluid flow is then simulated by describing the collision and streaming processes of particle distribution functions within the discrete phase space. By introducing a pseudopotential to model interparticle forces, Shan and Chen (1993) modified the LBM for multiphase flow applications. In this study, a multiple-relaxation-time lattice Boltzmann model proposed in our previous work (Wang et al., 2022), which has been validated using the Laplace law and contact angle tests, is employed to simulate oil-water flow. The governing evolution equation is expressed as follows:

$$f_{i,\alpha}(\mathbf{x}+\mathbf{e}_\alpha\delta_t, t+\delta_t) - f_{i,\alpha}(\mathbf{x},t) = -\mathbf{M}^{-1}\mathbf{\Lambda}\mathbf{M}\left(f_{i,\beta}(\mathbf{x},t) - f^{\mathrm{eq}}_{i,\beta}(\mathbf{x},t)\right) + \delta_t F_{i,\alpha} \tag{3}$$

where $\mathbf{x}$ position and time t, and $\alpha = 0, 1, 2, \ldots, 8$ are the nine directions of the D2Q9 model, $f_{i,\alpha}(\mathbf{x}, t)$ refers to the i-component particle distribution function in the discrete space, δ_t denotes the time step, $\mathbf{e}_\alpha$ represents the velocity at α direction, $\mathbf{\Lambda}$ is the relaxation diagonal matrix, F_α is the external force at α direction, and $\mathbf{M}$ indicates the transformation matrix, which is given as:

$$\mathbf{M} = \begin{bmatrix} 1 & 1 & 1 & 1 & 1 & 1 & 1 & 1 & 1 \\ -4 & -1 & -1 & -1 & -1 & 2 & 2 & 2 & 2 \\ 4 & -2 & -2 & -2 & -2 & 1 & 1 & 1 & 1 \\ 0 & 1 & 0 & -1 & 0 & 1 & -1 & -1 & 1 \\ 0 & -2 & 0 & 2 & 0 & 1 & -1 & -1 & 1 \\ 0 & 0 & 1 & 0 & -1 & 1 & 1 & -1 & -1 \\ 0 & 0 & -2 & 0 & 2 & 1 & 1 & -1 & -1 \\ 0 & 1 & -1 & 1 & -1 & 0 & 0 & 0 & 0 \\ 0 & 0 & 0 & 0 & 0 & 1 & -1 & 1 & -1 \end{bmatrix} \tag{4}$$

The relaxation diagonal matrix $\mathbf{\Lambda}$ is defined as:

$$\mathbf{\Lambda} = \mathrm{diag}(s_0, s_1, s_2, s_3, s_4, s_5, s_6, s_7, s_8) \tag{5}$$

where $s_7 = s_8 = s_\upsilon = 1/\tau$, determine the dimensional kinematic viscosity, τ is relaxation time and $\tau = \upsilon/(c^2_s{\cdot}\delta_t) + 0.5$. υ is kinematic viscosity, and $c_s = 1/\sqrt{3}$ expresses the sound speed.

The $\mathbf{F}_\sigma = \mathbf{F}_{\sigma,\mathrm{int}} + \mathbf{F}_{\sigma,\mathrm{ads}} + \mathbf{F}_{\sigma,\mathrm{b}}$ is total force, and $\mathbf{F}_{\sigma,\mathrm{int}}$ describes the liquid-liquid interaction force, $\mathbf{F}_{\sigma,\mathrm{ads}}$ is defined as the liquid-solid interaction force, and $\mathbf{F}_{\sigma,\mathrm{b}}$ is the external body force.

Prior to the simulation, the pore-throat system is fully saturated with the oil phase. The left boundary of the model serves as the inlet for the water phase, whereas the right boundary functions as the outlet for the oil phase. The Periodic boundary conditions are applied in simulating the forced imbibition of water phase. The contact angle is set to 40°. The simulation is conducted for a total of 2,500,000 time steps. Furthermore, previous studies indicate that capillary forces dominate the imbibition process in shale (Hu et al., 2019; Ding et al., 2022), while external fluid pressure is applied during the imbibition experiments. Therefore, osmotic pressure is not considered in the LBM simulations of fluid flow.

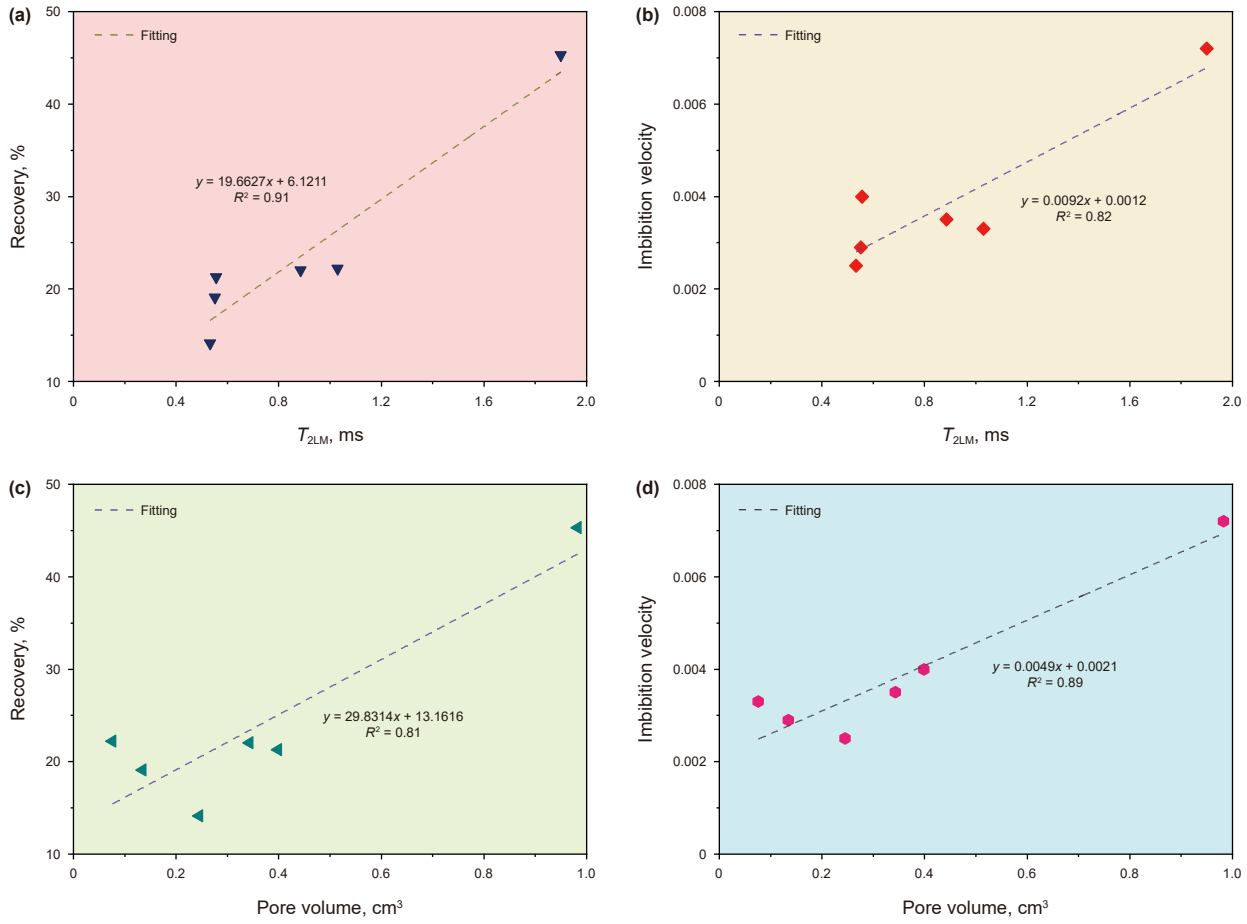

Fig. 7. Relationships between pore structure parameters and imbibition behavior. **(a)** T_{2LM} with recovery, **(b)** T_{2LM} with imbibition velocity, **(c)** pore volume with recovery, **(d)** pore volume with imbibition velocity.

4.3.4. Fluid distributions before and after clay swelling

Based on the lattice Boltzmann model developed above, forced imbibition of water phase is simulated for pore fracture structures before and after clay swelling. The results indicate pronounced differences in fluid distribution and transport mechanisms under the various imbibition stages, as shown in Fig. 10. At the initial stage, the water phase gradually invades the pore space without passing through the clay swelling region. As the wetting phase, the water interface assumes a meniscus shape, with the capillary force directed toward the oil phase (Fig. 10(a) and (d)). With further fluid injection, the water phase penetrates more extensively into the porous medium, where the complex internal geometric structure of shale facilitates the formation of preferential flow pathways. When compared with the network after swelling (Fig. 10(e)), the unaltered structure contains more preferential flow channels (Fig. 10(b)), promoting a wider swept of the water phase and consequently resulting in a lower residual oil saturation. Additionally, by focusing on the region of clay mineral, the influence of clay swelling on oil water distribution is further revealed. Under the compression induced by clay swelling, the sizes of pores and throats decrease, and the number of dead-end pores increases. Due to the existence of dead-end pores (Fig. 10(e1)), part of the oil phase cannot move through the original throats and remains confined within these pores. The swelling of clay also enhances the Jamin effect in constricted throats (Fig. 10(e2)), which results in high resistance to the oil phase and traps oil droplets within the pore space.

The appearance of water at the outlet of the porous media model indicates that the forced imbibition process has reached the breakthrough stage (Fig. 10(c) and (f)). The impact of clay swelling on fluid distribution is particularly pronounced at this stage: the quantity of dominant flow paths decreases sharply, directly resulting in substantial oil phase being trapped within the core. The microscopic investigation of the local clay region further demonstrates that throat closure due to swelling reshapes the water phase flow pathway (Fig. 10(c1) and (f1)), resulting in a more restricted path for forced imbibition. Water preferentially invades along the walls due to throat constriction. As a result, the oil phase is broken into small droplets at the throats (Fig. 10(f2)), a phenomenon known as snap-off (Singh et al., 2022; Cai et al., 2024). By disrupting the continuity of the oil phase, snap-off substantially increases flow resistance, confining oil within the pores and reducing the overall recovery.

With sustained fluid injection, the oil phase becomes immobilized within the pore fracture structure, entering the residual oil stage in which recovery stabilizes (Fig. 11(a)). Similarly, owing to the reduced pore connectivity and diminished pore sizes, the structure after swelling retains a greater number of residual oil droplets in the final stage. By quantifying the oil production at the outlet, the variation in recovery with imbibition time is obtained (Fig. 11(b)). The imbibition rate of the structure with clay swelling is clearly lower than that of the original configuration, in agreement with the results of the imbibition experiments. Clay swelling weakens the fluid transport capacity of the pore fracture system.

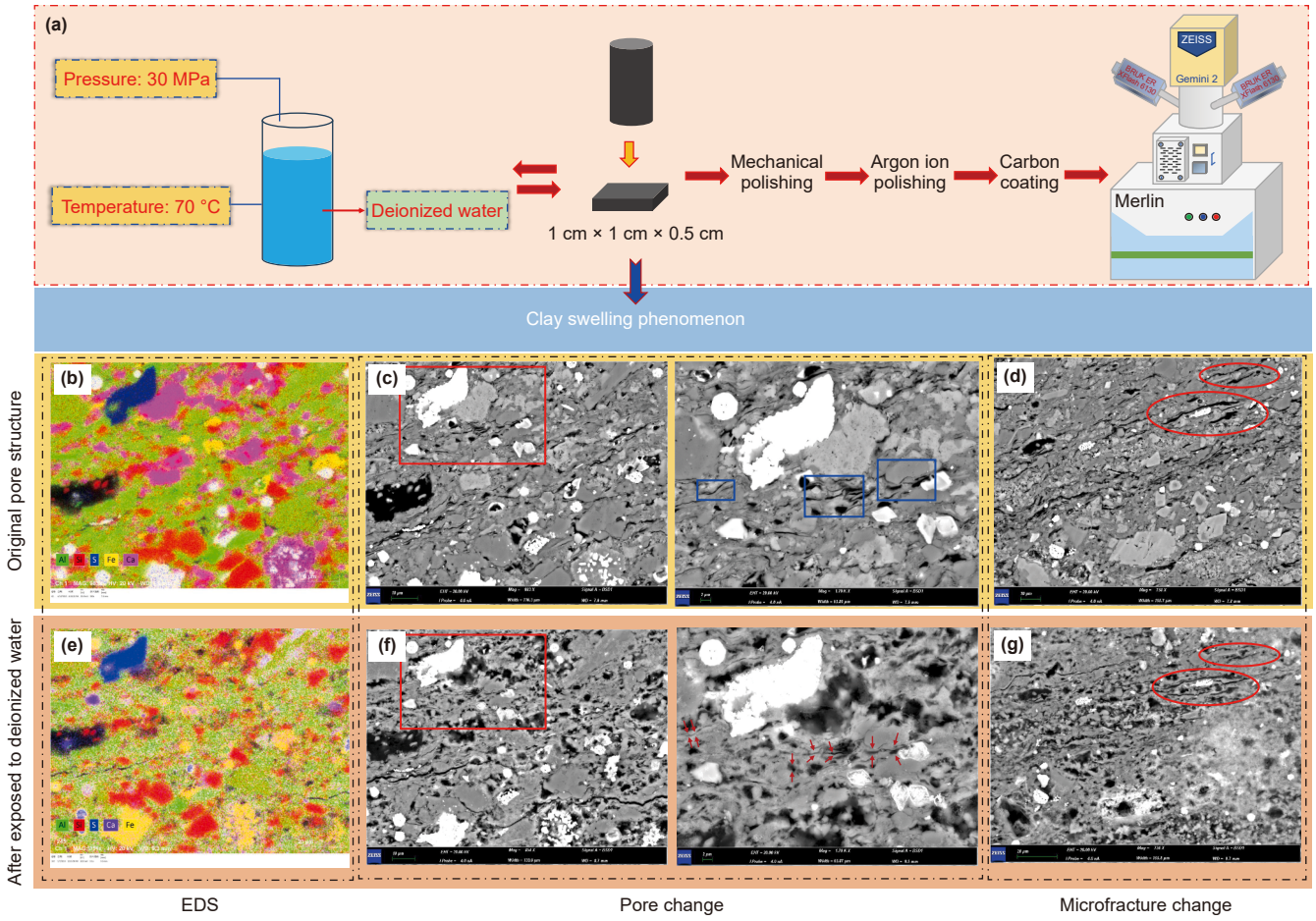

Fig. 8. SEM characterization of shale interacting with deionized water. **(a)** The experiment flowchart, **(b)** EDS from original sample, **(c)** original pore, **(d)** original microfracture, **(e)** EDS from swelling sample, **(f)** pore after swelling, **(g)** microfracture after swelling.

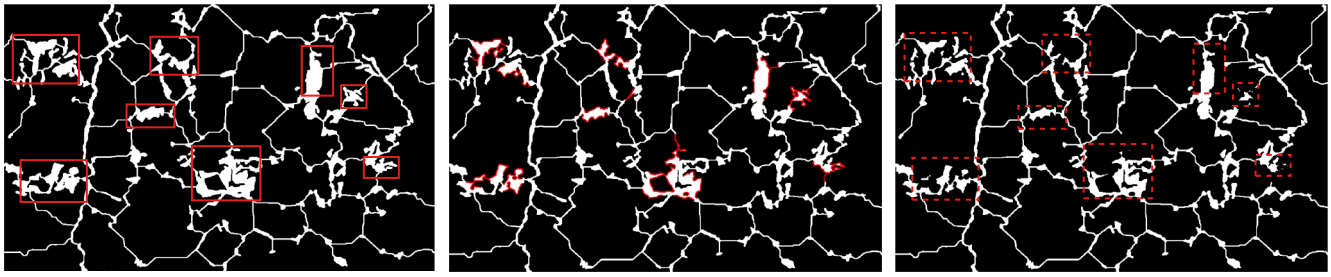

(a) Original pore structure **(b)** Swelling area **(c)** Pore structure after swelling

Fig. 9. The construction of the pore fracture structure incorporating clay swelling. **(a)** Original pore structure, **(b)** swelling area, **(c)** pore structure after swelling.

The original structure exhibits an imbibition recovery of 77.7%, which declines to 72.5% after clay swelling. This is consistent with the differences observed in the experiments, indicating that alterations in pore structure have a clear impact on imbibition recovery.

To explore how wettability affects fluid dynamics, forced imbibition simulations employ water contact angles of 40°, 50°, and 60°, guided by contact angle tests from systems with different salinities. At the same timestep, increasing the water-phase contact angle from 40° to 60° results in no discernible modification of the imbibition front (Fig. 12 (a)–(c)). The fluid distribution characteristics and flow pathways remain essentially unchanged under different wettability conditions. As shown in the recovery profiles for varying wettability (Fig. 12(d)), the recovery curves corresponding to contact angles of 40°, 50°, and 60° almost coincide throughout the entire imbibition period. In contrast to Fig. 11(b), the imbibition and diffusion of the water phase within the pore space show little dependence on variations in contact angle. Under different contact angle conditions, the final oil recovery remains nearly identical. The results demonstrate that the degree of wettability alteration caused by salinity differences in this study has a negligible impact on imbibition recovery. Therefore, it cannot be regarded as the principal driver of recovery variation.

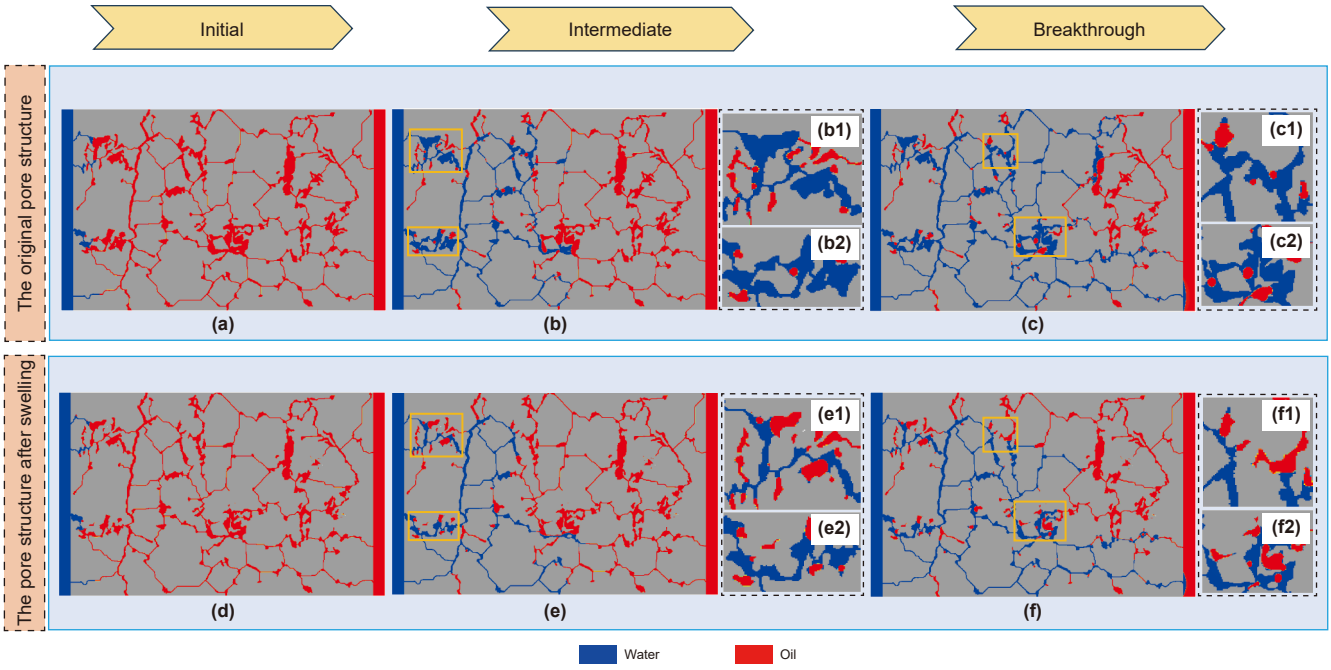

Fig. 10. Fluid distributions at different stage before and after clay swelling. Initial stage: **(a)**, **(d)**; intermediate stage: **(b)**, **(e)**; breakthrough stage: **(c)**, **(f)**.

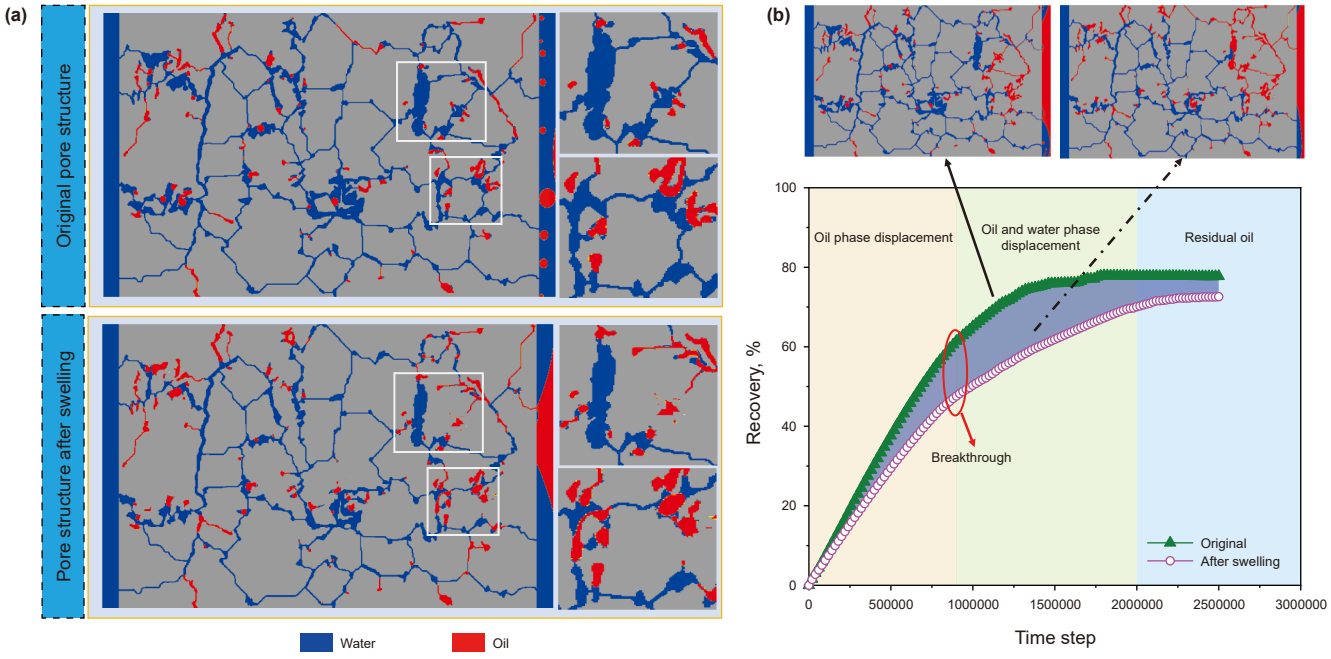

Fig. 11. The residual oil stage **(a)** and recovery curve **(b)**.

5. Conclusions

In this work, continental shale samples are examined using nuclear magnetic resonance to perform imbibition experiments with solutions of different salinities. The effects of salinities on imbibition behavior are analyzed based on transverse relaxation time spectra. Scanning electron microscopy is employed to provide microscopic insight of clay swelling. Lattice Boltzmann method simulations are used to elucidate how changes in pore structure induced by variations in salinity affect shale imbibition. The main conclusions are summarized as follows:

(1) The elevated capillary forces in small pores cause imbibition to occur preferentially in these regions, promoting the displacement of oil toward larger pores. This migration slightly enhances the signal amplitude of nuclear magnetic resonance corresponding to the large pores.

(2) Scanning electron microscopy observations verify that low salinity conditions induce clay swelling, which in turn compresses the surrounding pore space and microfracture. The dissolution pores formed by the detachment of carbonate minerals remain unconnected, exerting only a minor effect on fluid flow.

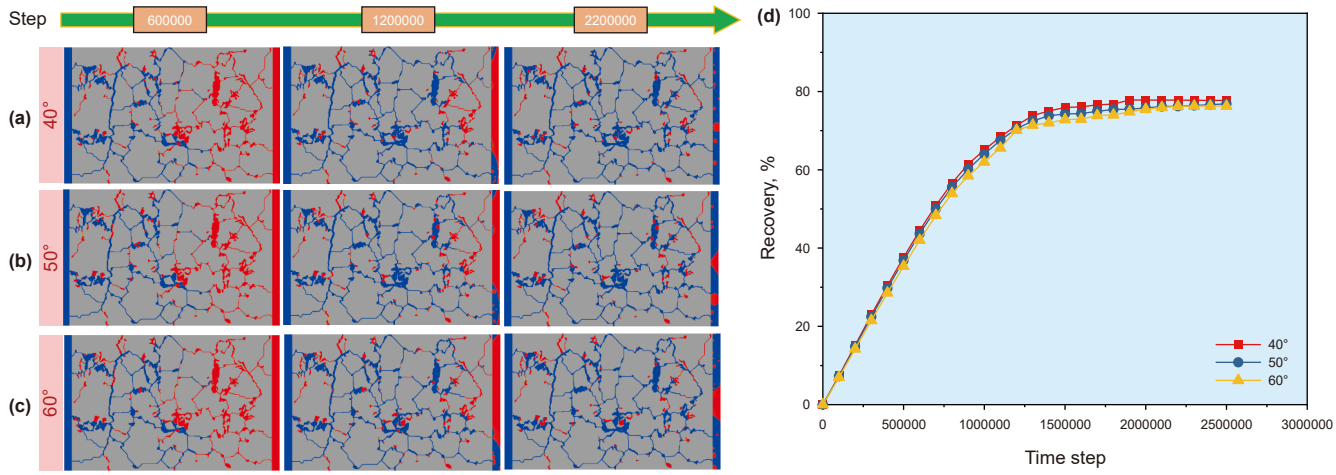

Fig. 12. Effect of wettability on imbibition behavior. **(a)** Water-phase contact angle of 40°, **(b)** water-phase contact angle of 50°, **(c)** water-phase contact angle of 60°, **(d)** recovery curves.

(3) Swelling of clay closes or constricts pore throats, limiting flow availability. The reduced throat apertures facilitate snap-off, causing the oil to break into discrete droplets that are subsequently trapped within the pore space, resulting in diminished oil recovery. High salinity effectively suppresses clay swelling and preserves pore connectivity, which constitutes the underlying reason for the enhanced imbibition recovery.

CRediT authorship contribution statement

Xuan-Zhe Xia: Writing – original draft, Investigation. **Ting Chen:** Data curation, Writing – review & editing. **Han Wang:** Writing – review & editing, Software, Funding acquisition. **Yu-Xuan Xia:** Writing – review & editing, Funding acquisition. **Liang Luo:** Funding acquisition, Writing – review & editing. **Jian-Chao Cai:** Writing – review & editing, Supervision, Funding acquisition.

Declaration of competing interest

The authors declare that they have no known competing financial interests or personal relationships that could have appeared to influence the work reported in this paper.

Acknowledgment

This work was supported by National Natural Science Foundation of China (Grant Nos. 42302143, 52404048, and 42172159).

References

Anderson, R.L., Ratcliffe, I., Greenwell, H.C., Williams, P.A., Cliffe, S., Coveney, P.V., 2010. Clay swelling – A challenge in the oilfield. Earth-Sci. Rev. 98 (3–4), 201–216. https://doi.org/10.1016/j.earscirev.2009.11.003.

Ashraf, S., Méheust, Y., Phirani, J., 2023. Spontaneous imbibition dynamics in two-dimensional porous media: A generalized interacting multi-capillary model. Phys. Fluids 35 (1), 012005. https://doi.org/10.1063/5.0123229.

Cai, J., Perfect, E., Cheng, C.L., Hu, X., 2014. Generalized modeling of spontaneous imbibition based on hagen-poiseuille flow in tortuous capillaries with variably shaped apertures. Langmuir 30 (18), 5142–5151. https://doi.org/10.1021/la5007204.

Cai, J., Qin, X., Xia, X., Jiao, X., Chen, H., Wang, H., Xia, Y., 2024. Numerical modeling of multiphase flow in porous media considering micro- and nanoscale effects: A comprehensive review. Gas Sci. Eng. 131, 205441. https://doi.org/10.1016/j.jgsce.2024.205441.

Ding, Y., Liu, X., Liang, L., Xiong, J., Hou, L., 2022. Experimental and model analysis on shale spontaneous imbibition and its influence factors. J. Nat. Gas Sci. Eng. 99, 104462. https://doi.org/10.1016/j.jngse.2022.104462.

Dou, Z., Yang, Z., Dong, C., Li, H., Wang, Y., Hou, H., 2024. Rock physical evolution and microscopic flow mechanism of massive energy replenishment in tight oil reservoirs. Adv. Geo-Energy Res. 14 (1), 49–63. https://doi.org/10.46690/ager.2024.10.07.

Eltahan, E., Rego, F.B., Yu, W., Sepehrnoori, K., 2021. Impact of well shut-in after hydraulic-fracture treatments on productivity and recovery of tight oil reservoirs. J. Pet. Sci. Eng. 203, 108592. https://doi.org/10.1016/j.petrol.2021.108592.

Fritz, S.J., 1986. Ideality of clay membranes in osmotic processes: A review. Clays Clay Miner. 34 (2), 214–223. https://doi.org/10.1346/CCMN.1986.0340212.

Fu, C., Xu, X., Du, Y., Kou, X., 2024. Experimental study on the influence of pore structure on spontaneous imbibition in marine black shale. Capillarity 10 (3), 57–72. https://doi.org/10.46690/capi.2024.03.01.

Handy, L.L., 1960. Determination of effective capillary pressures for porous media from imbibition data. Petrol. Trans. AIME 219 (1), 75–80. https://doi.org/10.2118/1361-G.

Hu, Z., Duan, X., He, Y., Wu, J., Chang, J., Liu, L., Wu, K., Ma, Z., 2019. Influence of reservoir primary water on shale gas occurrence and flow capacity. Nat. Gas. Ind. B. 6 (1), 71–78. https://doi.org/10.1016/j.ngib.2019.01.010.

Huang, T., Cheng, L., Cao, R., et al., 2024. Molecular simulation of the dynamic distribution of complex oil components in shale nanopores during CO_2-EOR. Chem. Chem. Eng. J. 479, 147743. https://doi.org/10.1016/j.cej.2023.147743.

Khan, H.J., Spielman-Sun, E., Jew, A.D., Bargar, J., Kovscek, A., Druhan, J.L., 2021. A critical review of the physicochemical impacts of water chemistry on shale in hydraulic fracturing systems. Environ. Sci. Technol. 55 (3), 1377–1394. https://doi.org/10.1021/acs.est.0c04901.

Li, S., Liu, H., Wu, R., Cai, J., Xi, G., Jiang, F., 2022. Prediction of spontaneous imbibition with gravity in porous media micromodels. J. Fluid Mech. 952, A9. https://doi.org/10.1017/jfm.2022.890.

Lin, Z., Hu, Q., Yin, N., Yang, S., Liu, H., Chao, J., 2024. Nanopores-to-microfractures flow mechanism and remaining distribution of shale oil during dynamic water spontaneous imbibition studied by nmr. Geoenergy Sci. Eng. 241, 213202. https://doi.org/10.1016/j.geoen.2024.213202.

Liu, J., Sheng, J.J., 2020. Investigation of countercurrent imbibition in oil-wet tight cores using NMR technology. SPE J. 25 (5), 2601–2614. https://doi.org/10.2118/201099-pa.

Lucas, R., 1918. Rate of capillary Ascension of liquids. Kolloid Z. 23, 15–22. https://doi.org/10.1007/BF01461107.

Lyu, C., Ning, Z., Chen, M., Wang, Q., 2019. Experimental study of boundary condition effects on spontaneous imbibition in tight sandstones. Fuel 235, 374–383. https://doi.org/10.1016/j.fuel.2018.07.119.

Maillet, B., Sidi-Boulenouar, R., Coussot, P., 2022. Dynamic NMR relaxometry as a simple tool for measuring liquid transfers and characterizing surface and structure evolution in porous media. Langmuir 38 (49), 15009–15025. https://doi.org/10.1021/acs.langmuir.2c01918.

Mattax, C.C., Kyte, J., 1962. Imbibition oil recovery from fractured, water-drive reservoir. SPE J. 2 (2), 177–184. https://doi.org/10.2118/187-PA.

Meng, M., Ge, H., Ji, W., Wang, X., Chen, L., 2015. Investigation on the variation of shale permeability with spontaneous imbibition time: Sandstones and volcanic rocks as comparative study. J. Nat. Gas Sci. Eng. 27, 1546–1554. https://doi.org/10.1016/j.jngse.2015.10.019.

Middleton, R.S., Gupta, R., Hyman, J.D., Viswanathan, H.S., 2017. The shale gas revolution: Barriers, sustainability, and emerging opportunities. Appl. Energy 199, 88–95. https://doi.org/10.1016/j.apenergy.2017.04.034.

Mitra, P.P., Sen, P.N., Schwartz, L.M., Le Doussal, P., 1992. Diffusion propagator as a probe of the structure of porous media. Phys. Rev. Lett. 68 (24), 3555. https://doi.org/10.1103/PhysRevLett.68.3555.

Mu, Y., Zou, C., Hu, Z., Duan, X., Guo, Q., Jing, Z., 2025. Impacts of multi-scale water-rock interaction on mineral alteration, mechanical weakening and pore-fracture evolution in marine shales. Adv. Geo-Energy Res. 17 (1), 68–81. https://doi.org/10.46690/ager.2025.07.06.

Munarin, F.F., Gouze, P., Filho, F.N., 2025. Two-phase flow dynamics in 3D fractures: Influence of aperture, wettability, and fluid properties from lattice Boltzmann simulations. Adv. Water Resour. 206, 105133. https://doi.org/10.1016/j.advwatres.2025.105133.

Murtaza, M., Allowaim, M., Rana, A., Kamal, M.S., Alarifi, S., Patel, S., Mahmoud, M., 2024. Comprehensive assessment of inorganic salt inhibitors for clay swelling mitigation in drilling and completion operations. In: SPE Conference at Oman petroleum & Energy Show. https://doi.org/10.2118/218563-ms.

Peng, S., Xiao, X., 2017. Investigation of multiphase fluid imbibition in shale through synchrotron-based dynamic micro-CT imaging. J. Geophys. Res. Solid Earth 122 (6), 4475–4491. https://doi.org/10.1002/2017jb014253.

Qin, X., Wang, H., Xia, Y., Jiao, X., Wang, G., Cai, J., 2025. Pore-scale investigation of water-CO_2-oil flow in shale fractures for enhanced displacement efficiency and CO_2 sequestration. Eng. Geol. 348, 107969. https://doi.org/10.1016/j.enggeo.2025.107969.

Shan, X., Chen, H., 1993. Lattice Boltzmann model for simulating flows with multiple phases and components. Phys. Rev. E. 47 (3), 1815–1819. https://doi.org/10.1103/PhysRevE.47.1815.

Shao, J., You, L., Jia, N., Kang, Y., Chen, M., 2023. Investigation of induced change in pore structure by the reaction of shale with fracturing fluid. Gas Sci. Eng. 110, 204860. https://doi.org/10.1016/j.jgsce.2022.204860.

Shen, Y., Ge, H., Li, C., Yang, X., Ren, K., Yang, Z., Su, S., 2016. Water imbibition of shale and its potential influence on shale gas recovery—A comparative study of marine and continental shale formations. J. Nat. Gas Sci. Eng. 35, 1121–1128. https://doi.org/10.1016/j.jngse.2016.09.053.

Singh, K., Bultreys, T., Raeini, A.Q., Shams, M., Blunt, M.J., 2022. New type of pore-snap-off and displacement correlations in imbibition. J. Colloid Interface Sci. 609, 384–392. https://doi.org/10.1016/j.jcis.2021.11.109.

Sui, W., Tian, Y., Yao, C., 2018. Investigation of microscopic pore structure variations of shale due to hydration effects through SEM fixed-point observation experiments. Petrol. Explor. Dev. 45 (5), 955–962. https://doi.org/10.1016/s1876-3804(18)30099-5.

Sun, M., Fu, J., Wang, Q., Gao, Z., 2024. Pore network characterization and fluid occurrence of shale reservoirs: state-of-the-art and future perspectives. Adv. Geo-Energy Res. 12 (3), 161–167. https://doi.org/10.46690/ager.2024.06.01.

Wang, G., Jiang, C., Shen, J., Han, D., Qin, X., 2019. Deformation and water transport behaviors study of heterogenous coal using CT-based 3D simulation. Int. J. Coal Geol. 211, 103204. https://doi.org/10.1016/j.coal.2019.05.011.

Wang, H., Wang, W., Su, Y., Jin, Z., 2022. Lattice Boltzmann model for oil/water two-phase flow in nanoporous media considering heterogeneous viscosity, liquid/solid, and liquid/liquid slip. SPE J. 27 (6), 3508–3524. https://doi.org/10.2118/210564-PA.

Wang, H., Zhang, M., Xia, X., Tian, Z., Qin, X., Cai, J., 2024. Lattice Boltzmann prediction of CO_2 and CH_4 competitive adsorption in shale porous media accelerated by machine learning for CO_2 sequestration and enhanced CH_4 recovery. Appl. Energy 370, 123638. https://doi.org/10.1016/j.apenergy.2024.123638.

Wang, L., Wang, H., Xia, X., Zhao, F., Masoodi, R., Xia, Y., 2025a. The effects of clay minerals on imbibition in shale reservoirs: A review. Capillarity 14 (1), 13–22. https://doi.org/10.46690/capi.2025.01.02.

Wang, Y.-J., You, L.-J., Yang, J., Kang, Y.-L., Chen, M.-J., Bai, J.-J., Tian, J., 2025b. Adsorption and retention of fracturing fluid and its impact on gas transport in tight sandstone with different clay minerals. Pet. Sci. 22 (1), 370–383. https://doi.org/10.1016/j.petsci.2024.09.012.

Wang, Y., Liu, X., Liang, L., Xiong, J., 2020. Experimental study on the damage of organic-rich shale during water-shale interaction. J. Nat. Gas Sci. Eng. 74, 103103. https://doi.org/10.1016/j.jngse.2019.103103.

Washburn, E.W., 1921. The dynamics of capillary flow. Phys. Rev. 17 (3), 273–283. https://doi.org/10.1103/PhysRev.17.273.

Wu, J., Yang, S., Li, Q., Huang, C., Wang, Z., Zhou, W., Chapman, S., Colledge, M., 2024. New insight into imbibition micromechanisms and scaling model in fossil hydrogen energy development of tight reservoirs based on NMR. Int. J. Hydrogen Energy 49, 964–977. https://doi.org/10.1016/j.ijhydene.2023.10.006.

Yang, L., Dou, N., Lu, X., Zhang, X., Chen, X., Gao, J., Yang, C., Wang, Y., 2018. Advances in understanding imbibition characteristics of shale using an NMR technique: A comparative study of marine and continental shale. J. Geophys. Eng. 15 (4), 1363–1375. https://doi.org/10.1088/1742-2140/aaaf76.

Yang, Y., Wang, S., Feng, Q., Cao, X., Qin, Y., Shu, C., Zhong, A., Wang, X., 2023. Imbibition mechanisms of fracturing fluid in shale oil formation: A review from the multiscale perspective. Energy Fuels 37 (14), 9822–9840. https://doi.org/10.1021/acs.energyfuels.3c00502.

Yao, Y., Sun, X., Zheng, S., Wu, H., Zhang, C., Liu, Y., Chang, Y., 2021. Methods for petrological and petrophysical characterization of gas shales. Energy Fuels 35 (14), 11061–11088. https://doi.org/10.1021/acs.energyfuels.1c01475.

Zeng, F., Zhang, Q., Guo, J., Zeng, B., Zhang, Y., He, S., 2021. Mechanisms of shale hydration and water block removal. Petrol. Explor. Dev. 48 (3), 752–761. https://doi.org/10.1016/s1876-3804(21)60061-7.

Zhang, J., Zhang, R., Ataceri, I., Sarmah, A., Schechter, D., Gildin, E., 2024. Enhancing oil recovery in eagle ford shale: A multiscale simulation study of surfactant huff 'n' puff methodology. SPE J. 29 (12), 7180–7193. https://doi.org/10.2118/223602-pa.

Zhang, L., Wei, Z., Xu, C., Ping, J., Imani, G., Sun, H., Fan, D., Fu, S., Hou, L., Yang, Y., Yao, J., 2025. A mathematical model and digital rock simulation of spontaneous imbibition in shale fracture-matrix systems. Phys. Fluids 37 (8), 083602. https://doi.org/10.1063/5.0278553.

Zhao, J., Wang, J., Zhang, G., Zhou, D., Chen, L., Viswanathan, H., Kang, Q., 2023. Minireview on lattice Boltzmann modeling of gas flow and adsorption in shale porous media: progress and future direction. Energy Fuels 37 (3), 1511–1524. https://doi.org/10.1021/acs.energyfuels.2c03298.

Zhao, W., Hu, S., Hou, L., Yang, T., Li, X., Guo, B., Yang, Z., 2020. Types and resource potential of continental shale oil in China and its boundary with tight oil. Petrol. Explor. Dev. 47 (1), 1–11. https://doi.org/10.1016/s1876-3804(20)60001-5.

Zheng, L., Wang, H., Jiang, J., Xiao, W., Zhu, B., Bernabé, Y., Zhang, J., 2025. A NMR investigation of spontaneous and forced imbibition of shale under different flow and confinement conditions. Capillarity 14 (2), 53–62. https://doi.org/10.46690/capi.2025.02.02.

Zuo, M.-S., Chen, H., Liu, X.-L., Liu, H.-P., Wu, Y., Qi, X.-Y., 2024. Fractal model of spontaneous imbibition in low-permeability reservoirs coupled with heterogeneity of pore seepage channels and threshold pressure. Pet. Sci. 21 (2), 1002–1017. https://doi.org/10.1016/j.petsci.2023.10.027.